THE JOURNAL OF BIOLOGICAL CHEMISTRY VOL. 289, NO. 14, pp. 9683–9691, April 4, 2014
Published in the U.S.A.

Myristoylation Restricts Orientation of the GRASP Domain on Membranes and Promotes Membrane Tethering*[S]

Received for publication, December 16, 2013, and in revised form, February 3, 2014 Published, JBC Papers in Press, February 6, 2014, DOI 10.1074/jbc.M113.543561

Frank Heinrich[‡§], **Hirsh Nanda**[‡§], **Haw Zan Goh**[‡1], **Collin Bachert**[¶], **Mathias Lösche**[‡§‖2], **and Adam D. Linstedt**[¶3]

From the Departments of [‡]*Physics,* [¶]*Biological Sciences, and* [‖]*Biomedical Engineering, Carnegie Mellon University, Pittsburgh, Pennsylvania 15213 and the* [§]*National Institute of Standards and Technology (NIST) Center for Neutron Research, Gaithersburg, Maryland 20899*

Background: An unknown mechanism promotes *trans* interactions by the GRASP homotypic membrane tethers rather than unproductive *cis* interactions.
Results: Neutron reflection shows that the myristoylated GRASP domain has a fixed, upright orientation on the membrane incompatible with *cis* interactions.
Conclusion: Myristoylation restricts the orientation of the protein on the membrane to favor interactions in *trans*.
Significance: Orientation of membrane proteins is functionally significant and may be regulated by myristoylation.

The mammalian Golgi reassembly stacking protein (GRASP) proteins are Golgi-localized homotypic membrane tethers that organize Golgi stacks into a long, contiguous ribbon-like structure. It is unknown how GRASPs undergo *trans* pairing given that *cis* interactions between the proteins in the plane of the membrane are intrinsically favored. To test the hypothesis that myristoylation of the self-interacting GRASP domain restricts its orientation on the membrane to favor *trans* pairing, we established an *in vitro* assay that recapitulates GRASP-dependent membrane tethering and used neutron reflection under similar conditions to determine the orientation of the GRASP domain. *In vivo*, the membrane association of GRASP proteins is conferred by the simultaneous insertion of an N-terminal myristic acid and binding to a Golgi-associated binding partner. In our assay, the latter contact was replaced using a C-terminal hexa-His moiety, which bound to Ni^{2+}-conjugated lipids incorporated into a substrate-supported bilayer lipid membrane. Non-myristoylated protein lacked a fixed orientation on the membrane and inefficiently tethered liposomes. In contrast, myristoylated GRASP promoted tethering and exhibited a unique membrane complex. Thus, myristoylation restricts the membrane orientation of the GRASP domain favoring interactions in *trans* for membrane tethering.

Proteins interact to bridge two adjacent membranes in many important cellular processes including cell-cell adhesion, virus-membrane attachment, vesicle docking, and organelle fusion (1–4). Such cross-bridging may be either homotypic or heterotypic depending on whether the process involves the pairing of self-interacting molecules or the pairing of distinct components on each of the apposed membranes. Uniquely, in these types of molecular interactions, the effectiveness of pairing is governed by the relative propensity of the proteins to form interactions in a *trans* configuration across the membranes, *versus* binding in *cis* in the same membrane. Particularly in the case of homotypic cross-bridging where *cis* interactions may predominate, a mechanism is needed to suppress such *cis* pairing.

An important example of homotypic tethering is the interaction of the GRASP[4] proteins that underlies stacking Golgi cisternae and/or linking the stacks into the elongated, ribbon-like membrane network evident in mammalian cells (5–9). GRASP65 is localized to *cis* Golgi cisternae, and GRASP55 is localized to *medial* and *trans* cisternae. The immediate effect of inhibiting GRASP65 is a loss of lateral continuity of *cis* cisternae, whereas inhibiting GRASP55 first disrupts *trans* cisternal continuity (10). Each GRASP protein contains two noncanonical PDZ domains and an internal PDZ ligand that protrudes from the surface of the molecule (11). Self-association occurs via the intermolecular insertion of the ligand into the binding groove of the first PDZ domain (12).

The GRASP proteins are anchored to their respective cisternal membranes by insertion of an N-terminal myristic acid and interaction of the second PDZ domain, which is positioned near the C terminus of the GRASP domain, with a membrane-bound partner protein (13, 14). Such dual anchoring of GRASP is required not only for its stable membrane association but also

* This work was supported by a grant from Dr. Fred Gilman, Dean of the Carnegie Mellon University Mellon College of Science to the CMU Membrane Biophysics Group and National Institutes of Health Grants R01 GM0095549 (to A. D. L.) and R01 GM101647 (to M. L.).
[S] This article contains supplemental Figs. S1–S13 and Tables S1–S4.
[1] Present address: School of Materials Science and Engineering, Nanyang Technological University, Singapore 639798.
[2] To whom correspondence may be addressed: Dept. of Physics, Carnegie Mellon University, 5000 Forbes Ave., Pittsburgh, PA 15213. E-mail: quench@cmu.edu.
[3] To whom correspondence may be addressed: Dept. of Biological Sciences, Carnegie Mellon University, 4400 5th Ave., Pittsburgh, PA 15213. E-mail: linstedt@andrew.cmu.edu.

[4] The abbreviations used are: GRASP, Golgi reassembly stacking protein; G55, GRASP55(1–208)-His_6; myrG55, myristoylated G55; DOPC, 1,2-dioleoyl-*sn*-glycero-3-phosphocholine; LR-PE, 1,2-dioleoyl-*sn*-glycero-3-phosphoethanolamine-*N*-(lissamine rhodamine B sulfonyl) ammonium salt; Ni^{2+}-NTA-DGS, 1,2-dioleoyl-*sn*-glycero-3-[(*N*-(5-amino-1-carboxypentyl)-iminodiacetic-acid)succinyl] nickel salt; HC18, Z 20-(Z-octadec-9-enyloxy)-3,6,9,12,15,18,22-heptaoxatetracont-31-ene-1-thiol; stBLM, sparsely tethered bilayer lipid membrane; NR, neutron reflection; CVO, component volume occupancy; DOPC, 1,2-dioleoyl-*sn*-glycero-3-phospho-choline; MD, molecular dynamics.

Downloaded from http://www.jbc.org/ by guest on August 29, 2018

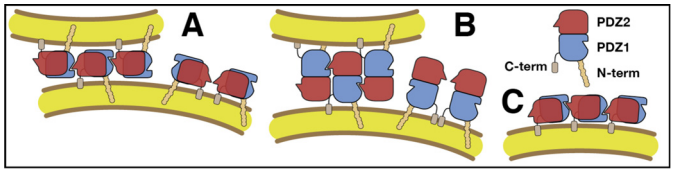

FIGURE 1. **Possible orientations of the GRASP domain, composed of PDZ1 (*blue*) and PDZ2 (*red*), and their implications on the protein's predilection for *trans* membrane tethering or unproductive *cis* protein binding.** The GRASP crystal structure shows that the groove on PDZ1, which accepts the internal ligand located on PDZ2, is on the opposite face of the GRASP domain from the internal ligand on PDZ2 (11). *A*, GRASP may lie flat on the membrane with the PDZ1 groove oriented coplanar while two membrane anchors keep the binding groove and the internal ligand rigidly in an orientation such that *cis* interactions become unlikely, as shown on the *right* of the lower membrane. *B*, a similar restriction to *cis* interactions would be achieved by an orientation in which GRASP sits upright on the membrane with one PDZ domain membrane bound and the other located distal from the membrane. The PDZ1 groove is oriented roughly coplanar, but *cis* interactions are unlikely because the PDZ groove and internal ligand are located at different distances from the membrane surface, and misoriented with respect to each other (*right side* on lower membrane). The membrane-membrane distance in this scenario is expected to be larger than for the GRASP orientations shown in *A*. *C*, if one of the two membrane anchors is compromised, the increased orientational flexibility of the GRASP domain leads to many other mutual orientations of the membrane-bound protein that will not discriminate between *cis* and *trans* binding, and hence result in many unproductive *cis* ligations. *C-term*, C terminus; *N-term*, N terminus.

for its membrane-tethering activity. Stable, singly anchored versions of GRASP proteins have been created using transmembrane domains but, when expressed in cells, they fail to tether, whereas similar dually anchored constructs retain full activity (12, 15). The singly anchored constructs are recovered in complexes, suggesting that they form *cis* interactions within the same membrane that are unproductive for tethering (15).

The relative positions of the internal ligand and the PDZ1 binding groove on the molecule (11) suggest that GRASP orientation on the membrane could provide a mechanism that favors homotypic interactions in *trans* over those in *cis* (15). However, for such a mechanism to work, the orientation of the protein with respect to the membrane needs to be tightly controlled, raising the possibility that *N*-myristoylation, as a second anchor point for the protein on the membrane, could set this orientation. Fig. 1 shows possible GRASP orientations on the membrane and their implications for forming *trans* or *cis* interactions. Many orientations will not prevent *cis* interactions from occurring, whereas some that do are fundamentally different but cannot be discriminated in functional assays.

Because orientation is difficult to determine *in vivo*, we developed an *in vitro* assay of GRASP-mediated tethering on sparsely tethered bilayer lipid membranes (stBLMs) where protein orientation can be determined with neutron scattering. The results show that the GRASP domain is sufficient for membrane tethering and that myristoylation is required for full activity. Neutron reflection revealed decisive differences in GRASP membrane orientation conferred by myristoylation, yielding a model of how orientation promotes *trans*-membrane tethering.

EXPERIMENTAL PROCEDURES

Materials—1,2-Dioleoyl-*sn*-glycero-3-phospho-choline (DOPC), 1,2-dioleoyl-*sn*-glycero-3-phos-phoethanolamine-*N*-(lissamine rhodamine B sulfonyl) ammonium salt (LR-PE), 1,2-dioleoyl-*sn*-glycero-3-[(*N*-(5-amino-1-carboxy-pentyl)imino-di-acetic-acid)succinyl] nickel salt (Ni^{2+}-NTA-DGS), and a liposome extruder were from Avanti Polar Lipids (Alabaster, AL) and used as prescribed. The tether lipid for supported membranes, Z 20-(Z-octadec-9-enyloxy)-3,6,9,12,15,18,22-heptaoxatetracont-31-ene-1-thiol (HC18) (17), was a generous gift from Dr. David Vanderah (Institute for Bioscience and Biotechnology Research, Rockville, MD). β-Mercaptoethanol was from Sigma-Aldrich. No. 1.5 glass coverslips were from Electron Microscopy Science (Hatfield, PA), and microscopy glass slides were from Fisher Scientific. All other chemicals were of HPLC grade. Ultrapure water was prepared in a Millipore (Billerica, MA) Milli-Q water purification device.

Constructs—GRASP55 was cloned into the pRSET-B vector by PCR amplification into the EcoRI site. Subsequently, the N-terminal His tag was deleted by a PCR loop-out procedure and a 10-amino acid linker, ASSRSGGSGA, after which a hexahistidine sequence was inserted after residue 208 followed by a stop codon to create G55, *i.e.* GRASP55(1–208)-His_6. The His_6-GRASP55(1–208) construct was made by PCR deletion of the His tag from GRASP55(1–208)-His_6 and reintroduction immediately before the starting methionine. Mutations of the pocket and ligand (L59A/I100S+Δ196–199) and of the phosphorylation site (S189D) were generated exactly as described previously (12, 18). The E157R mutation was subsequently introduced into the S189D construct using QuikChange according to the manufacturer's protocol (Stratagene, La Jolla, CA). All constructs were confirmed by sequencing. Protein was induced and myristoylated as described previously (12) to yield myrG55. Buffers used for protein incubation of interfaces in surface plasmon resonance (SPR), fluorescence microscopy, and neutron reflection (NR) contained 50 mmol/liter K_2HPO_4, adjusted to pH 7.45. The mitochondrial tethering assay was as described previously (12, 18).

Formation of stBLMs—stBLMs were formed on solid substrates as described previously (19, 20). The substrates, No. 1.5 glass coverslips or microscope glass slides for SPR and microscopy, respectively, and 3-inch (75-mm) silicon wafers (El-Cat Inc., Ridgefield Park, NJ) for NR, were thoroughly cleaned as described (21) and metal-coated by magnetron sputtering (ATC Orion, AJA International, Inc., North Scituate, MA). For fluorescence microscopy, ~6 nm of gold was sputtered on top of an ~2-nm thick chromium bonding layer, which leaves the coverslips optically transparent. For SPR, ~45 nm of gold was sputtered on the chromium bonding layer. Gold layers on chromium for NR were 10–15 nm thick. Freshly gold-coated substrates were immersed in an ethanolic solution of 30% HC18 and 70% β-mercaptoethanol, at a total concentration of 0.2 mmol/liter, to form a mixed self-assembly monolayer. Rapid solvent exchange (19, 22) or vesicle fusion was used to complete the formation of stBLMs.

Liposome Preparation—DOPC, together with 0.74 or 2.2 mol % LR-PE or 0.125 mol % Ni^{2+}-NTA-DGS as needed, was dissolved in chloroform in a vial and placed in vacuum to remove the solvent. The dry lipid films were redissolved in pentane and dried under vacuum again and then rehydrated in 50 mmol/liter potassium phosphate buffer at pH ~7.45 and sonicated. The resulting liposome suspensions were extruded through

Downloaded from http://www.jbc.org/ by guest on August 29, 2018

polycarbonate membranes with a pore size of 100 nm, and liposome sizes were checked by dynamic light scattering (Malvern Zetananosizer, Malvern Instruments Ltd., Malvern, UK). Alternate liposome sizes were also investigated (extrusion through 30- and 200-nm pore sizes; data not shown). 100 nm-extruded liposomes were used throughout the experiments shown in the study.

SPR—stBLMs formed on gold-coated microscope glass slides were mounted on a custom-made SPR instrument (SPR Biosystems, Germantown, MD) (21) in the Kretschmann configuration. A convergent fan of light (λ = 763.8 nm) was reflected from the backside of the sample-covered interface and recorded by a CCD chip, and the position of the intensity minimum was determined as a function of the reflection angle. Shifts in the resonance were used to quantify protein binding to the stBLM (21) after injection into the sample chamber. Resonance shifts as a function of protein concentration were fitted to a Langmuir isotherm to determine the dissociation constants, K_d.

Fluorescence Microscopy—stBLMs formed on gold-coated glass coverslip were assembled in a Sykes-Moore chamber. Subsequently, 1.2 μmol/liter protein and 0.01 mg/ml liposomes were injected into the chamber. The solution was occasionally mixed and left to incubate the stBLMs for 3 h before excess protein and liposomes were rinsed away. The chamber was then transferred to a Carl Zeiss Axiovert 200M microscope equipped with a Zeiss 63× Plan-Apochromat (NA = 1.4) objective lens, a 100-watt HBO 103 W/2 mercury lamp, a Zeiss filter set at BP546/12:FT560: BP665/20, and a Hamamatsu C9100-12 EM-CCD camera (Hamamatsu, Bridgewater, NJ) and controlled with IPLab (BioVision Technologies, Exton, PA). Images of LR-PE labeled liposomes adhering to the stBLMs were taken with ~300-ms exposure time at low excitation light intensity with the aperture stop closed to its minimum size. These image acquisition parameters were chosen to minimize the number of saturated pixels in the images. For each sample, at least 12 images (size of field, 100 × 100 μm^2) were taken at random positions in the sample. The fluorescence intensity of these images after background subtraction was used as a measure to quantify the tethering activity of the protein constructs.

Neutron Reflection Measurements and Data Modeling—NR measurements were performed on the NG7 and MAGIK reflectometers at the NIST Center for Neutron Research and evaluated with garefl (23) using the GRASP55 crystal structure (Protein Data Bank (PDB): 3RLE), similarly to studies of other membrane-associated proteins (21, 24). To determine the protein orientation on the membrane, the origins of the two relevant Euler angles (see Fig. 4*C*, *inset*) were chosen to coincide with the longest (ϑ_0) and second longest (φ_0) principal axes of the mass distribution in the crystal structure. Parameter space was efficiently searched with a Monte-Carlo Markov Chain algorithm, and provided quantitative measures of parameter and neutron scattering length density confidence limits, as well as parameter cross-correlations (25). The crystal structure used in the refinement was reported for a truncated protein, GRASP55(7–208), and also lacks the *N*-myristoylation and the C-terminal decapeptide and His tag. Therefore, this structure needed to be supplemented to represent the protein used in the experiments. Peptide conformations were obtained from molecular dynamics (MD) simulation. Because the protein orientation on the membrane was initially unknown, a first, free MD simulation of the full-length proteins in buffer sampled mostly unrealistic peptide conformations. However, this procedure produced an approximate full-length protein model that could be used to gain a first estimate of the protein orientation on the membrane through refinement to the NR data. Based on this orientation, we subsequently modified the model using a steered MD simulation to implement constraints of the His tag and the *N*-myristoylation reaching to the membrane surface. This refined model was then used to fit the NR data in a second round of modeling. In practical terms, both models yielded the same protein orientation and distance to the bilayer within confidence limits, and this structural protein model was used to determine a unique component volume occupancy profile as a parent of the neutron scattering length density profiles for different isotopic samples.

Molecular Modeling—Missing amino acids on the N and C termini of GRASP were added to the crystal structure in an initial fully extended configuration. The patched protein structure was modeled using the Generalized Born Implicit Solvent model implemented in NAMD 2.8 (26). A solvent dielectric of 78.5 and an ionic concentration of 0.1 mol/liter salt were used in the Generalized Born Implicit Solvent model. The resulting GRASP structure was minimized, first with the core protein held fixed and only the newly constructed termini allowed to vary. Then, in a second step of minimization, the full structure was allowed to vary. Further equilibration was performed with 10 ns of MD simulations followed by a 10-ns production run at 300 K. During both equilibration and production simulations, the backbone of the core protein was held fixed while the side chains were unrestrained. Both the backbone and the side chains of the added terminal residues were unrestrained. CHARMM22 with CMAP dihedral correction (27) was used for the protein force field parameters, and the CHARMM36 parameter set (28) was used for the myristate group on the N terminus. Frames were collected every 100 ps from the production run and averaged to generate the volume and scattering length profile of the GRASP protein that was then used for reflectivity fitting. Steered MD was performed on the N and C termini using the SMD module in NAMD. An external force was applied to the N-terminal Gly residue and the center of mass of the C-terminal His_6 tag. The force was directed downward along the *z* axis toward the putative membrane interface, resulting in a constant migration velocity of 0.0025 Å/fs.

RESULTS

GRASP Domain-mediated Liposome Tethering to Supported Membranes—To quantify the tethering activity of the GRASP domain *in vitro*, we developed a fluorescence-based assay that reports the tethering of liposomes to a supported planar bilayer. The aforementioned stBLMs feature a nanometer-thick hydrated layer between the solid surface and the lipid bilayer (19, 25) that keeps the bilayer in a physiologically relevant in-plane fluid state (29). We used purified preparations of the *N*-myristoylated and unmyristoylated GRASP domain of GRASP55 (residues 1–208). The resulting proteins, myrG55

Downloaded from http://www.jbc.org/ by guest on August 29, 2018

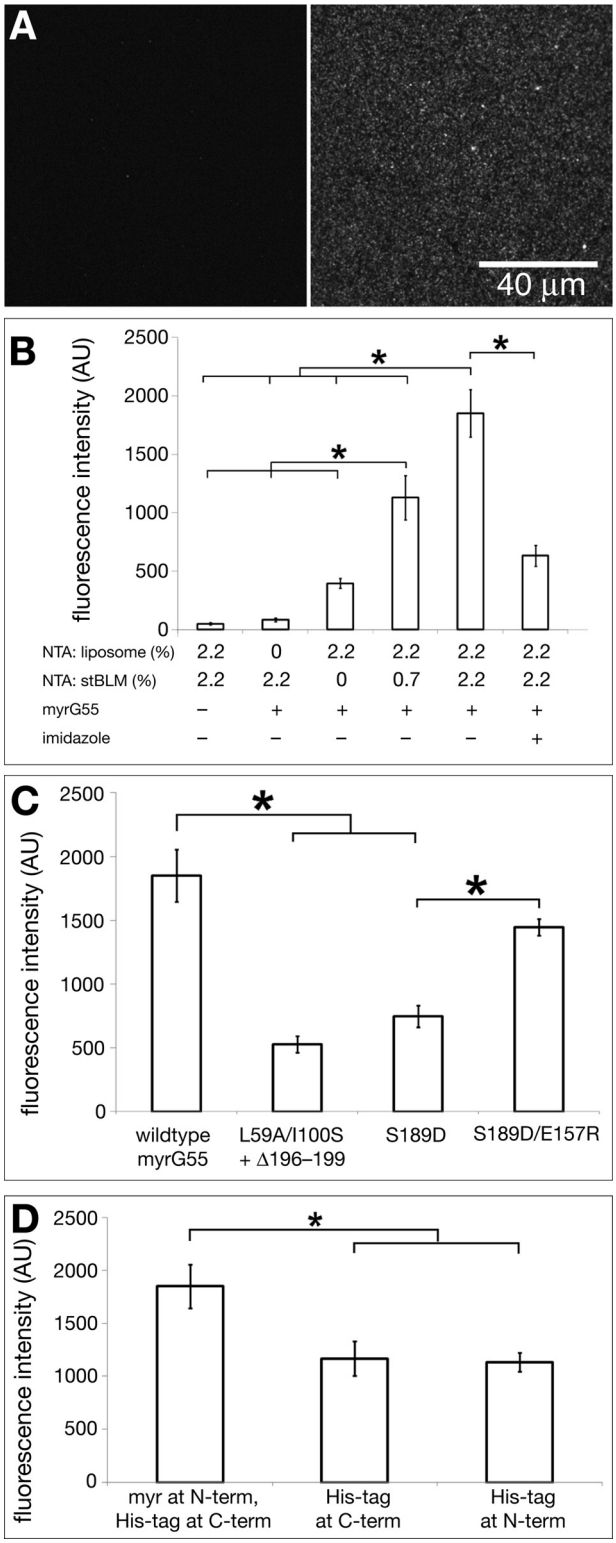

FIGURE 2. **Quantification of the GRASP55 GRASP domain tethering activity in an *in vitro* assay.** *A*, tethering of DOPC liposomes, doped with 0.125 mol % LR-DOPE, to HC18/DOPC stBLMs. Both liposomes and stBLMs contained 2.2 mol % Ni^{2+}-NTA-DGS. *Right*, liposomes tethered by myrG55 in a solution that contained 1.2 μmol/liter protein. Control (*left*) shows only a few vesicles nonspecifically absorbed to an stBLM in the absence of protein under otherwise identical conditions. *B*, interfacial fluorescence intensities of GRASP-tethered liposomes (1.2 μmol/liter myrG55), read out from the assay shown in *A*, at various concentrations of Ni^{2+}-NTA-DGS as indicated (*central four columns*). The *first* and the *last columns* show background (no protein) and remaining intensity after an imidazole (200 mmol/liter) wash, respectively. *AU*, arbitrary units. *C*, interfacial fluorescence intensity of tethered liposomes as in *B*, incubated in solutions that contained wild-type myrG55 or various mutants of this construct (see "Results"). *D*, relative tether efficiencies of the GRASP55 GRASP domain as a function of membrane anchor placement. Data in *panels A–D* are mean ± S.E. for $n \geq 3$ independent samples. *Asterisks* indicate one-tailed *p* values < 0.01.

and G55, included a 10-residue linker and C-terminal hexahistidine tag so that each protein bound to nickel (Ni^{2+}) associated with *N*-nitrilotriacetic acid (NTA)-functionalized lipids present in both the stBLMs and the liposomes in the assay. The C-terminal position of the His tag was meant to roughly approximate the position of the PDZ2 binding groove, which is near the C terminus of the GRASP domain and is normally responsible for the secondary site of membrane contact.

First, we determined the affinity of myrG55 to DOPC stBLMs containing 1 mol % Ni^{2+}-NTA-DGS using SPR. The reaction yielded a dissociation constant, K_d, of 0.32 ± 0.09 μmol/liter (data not shown) comparable with binding constants measured for other His-tagged proteins to Ni^{2+}-NTA-DGS (30, 31). The extrapolated ($c_{protein} \rightarrow \infty$) equilibrium SPR signal corresponded to a protein mass density of ~68 ng/cm^2, as calibrated with neutron reflection.[5] The background of nonspecific protein binding, quantified with myrG55 on DOPC stBLMs devoid of Ni^{2+}-NTA-DGS, was <10% of the signal with Ni^{2+}-NTA-DGS. This is consistent with the relatively weak affinity of myristate for the membrane, K_d ~100 μmol/liter (32), and with the inability of myristoylation alone to localize the GRASP proteins to membranes in cells (13, 15).

Next, we tested whether the GRASP domain construct was sufficient to tether vesicles to stBLMs. Liposomes, labeled with 0.125 mol % fluorescent LR-PE, and stBLMs were prepared from DOPC and varying amounts of Ni^{2+}-NTA-DGS. Liposomes (0.01 mg/ml) and myrG55 were incubated with stBLMs for 3 h after which excess protein and liposomes were rinsed off and the fluorescence intensity was determined at the interface (Fig. 2*A*). The background signal of the assay was established with stBLMs and liposomes (both with 2.2 mol % of Ni^{2+}-NTA-DGS) incubated without protein (Fig. 2*A*, *left*). With 1.2 μmol/liter myrG55, tethered liposomes (Fig. 2*A*, *right*) were observed with an intensity of >10× background that increased with Ni^{2+}-NTA-DGS concentration (Fig. 2*B*). A low level signal, ~4× background, was also observed in the presence of myrG55 when only liposomes, but not the stBLMs, contained Ni^{2+}-NTA-DGS. We attribute this increase in background over that measured without protein to GRASP-mediated tethering of liposomes in solution, resulting in higher fluorescence intensity upon nonspecific adsorption to the stBLMs. Indeed, large liposome aggregates, tens of μm across, were evident in the liposome suspension containing myrG55 after 3 h of incubation. Flushing tethered liposomes with 200 mmol/liter imidazole decreased the fluorescence intensity by a factor of ~3 (Fig. 2*B*), demonstrating further that liposome tethering is contingent on membrane-associated GRASP. Under the conditions of the experiment, imidazole may have had incomplete access to the preformed complexes accounting for the residual activity. Overall, the assay showed conclusively that the isolated GRASP

[5] F. Heinrich and H. Z. Goh, unpublished data.

Downloaded from http://www.jbc.org/ by guest on August 29, 2018

domain is capable of tethering membranes in the absence of any other factors.

Structural Requirements of GRASP Domain-mediated Tethering—To explore the mechanism of GRASP-mediated tethering, we used the *in vitro* assay to test three specific hypotheses that emerged from previous work carried out in cells. The first is that GRASP proteins tether Golgi membranes through an intermolecular self-interaction in which the internal ligand (residues 196–199) binds to the PDZ1 binding groove (11). Therefore, we mutated the GRASP domain construct by introducing known blocking substitutions into the PDZ1 binding groove (L59A/I100S) and deleting the residues of the internal ligand (Δ196–199). This construct was strongly blocked in its tethering activity (Fig. 2*C*, L59A/I100S+Δ196–199), suggesting that the previously identified binding interface mediates tethering in an assay devoid of other components.

The second hypothesis we tested is that mitotic phosphorylation of Ser-189 inhibits tethering by causing a conformational change in the internal ligand (33). Because the conformational change is evident in a crystal structure of the GRASP domain containing a phosphomimetic mutation, S189D, we tested this mutation in the assay and found that it significantly impaired tethering (Fig. 2*C*, S189D). Phosphorylation at Ser-189 is thought to disrupt an electrostatic contact between Ser-189 and Glu-157, thereby causing a rotation of the α2 helix that propagates to the ligand (33). Thus, in the double mutation S189D/E157R, the placement of Arg should re-establish, in the S189D background, the contact between residues 189 and 157 in wild-type GRASP, thereby reversing the conformational change and rescuing tethering activity. Indeed, the tethering activity of this construct was nearly restored to that of the wild-type protein (Fig. 2*C*, S189D/E157R). To confirm that these mutations similarly affect tethering activity *in vivo*, we used a previously characterized assay in which GRASP is targeted to mitochondria and the resulting tethering of the mitochondria is measured by the cellular fluorescence distribution (12). Indeed, despite being stably targeted to mitochondria, a version of full-length GRASP55 containing the S189D substitution was significantly impaired when compared with the corresponding wild-type version, and the double substitution S189D/E157R reversed this inhibition (Fig. 3).

The final test concerned *N*-myristoylation of GRASP, which is thought to be important not only for membrane targeting but also for membrane tethering (12, 15). Therefore, we compared the tethering activity of myrG55 with that of G55. Consistent with previous work in cell-based assays (12, 15), tethering activity was significantly lower in the absence of myristoylation (Fig. 2*D*, His tag at the C terminus). Because myristoylation is not essential for membrane anchoring of the His-tagged construct, this result suggests that *N*-myristoylation is required for efficient tethering. It is noteworthy that membrane association of the N terminus alone was ineffective as tethering activity remained at a reduced level if the His tag was moved from the C terminus to the N terminus (Fig. 2*D*, His tag at the N terminus). Thus, full tethering activity depends critically on simultaneous membrane anchoring of both termini of the GRASP domain, consistent with previous *in vivo* work.

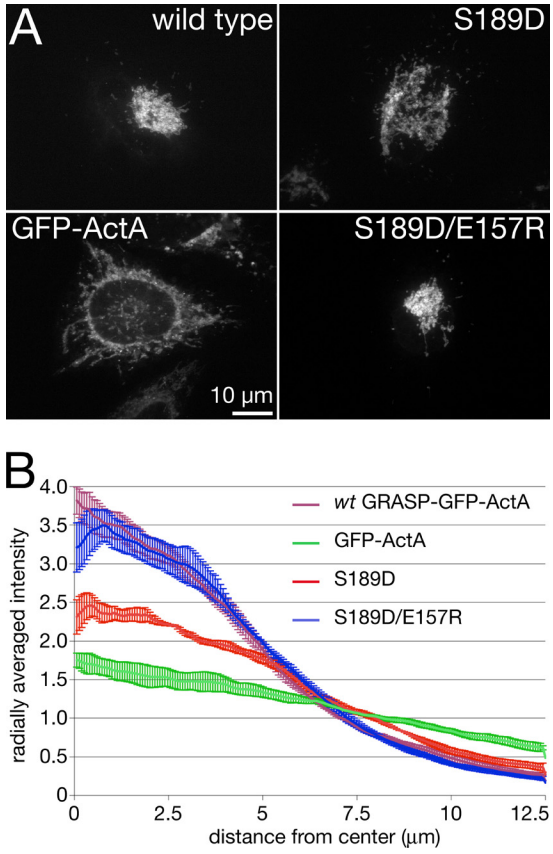

FIGURE 3. **GRASP-mediated membrane tethering of mitochondria.** *A*, HeLa cells expressing GFP-labeled proteins containing the ActA mitochondrial targeting sequence were analyzed 24 h after transfection. Cells were imaged using GFP fluorescence to identify transfected proteins. Representative GFP fluorescence patterns are shown for wild-type GRASP55, GRASP55 containing the S189D or S189D/E157R substitutions, and a control construct containing only the targeting signal (GFP-ActA). *B*, fluorescence distribution was quantified by radial profile analysis, which reports averages corresponding to the fraction of total fluorescence present in each concentric circle drawn from the centroid. Note that tethering activity is indicated by the degree of fluorescence near the centroid ($n = 3$, ± S.E., ≥15 cells per experiment).

Structure of the GRASP Domain Complex with the Membrane—To correlate the functional requirements for membrane tethering with structural details of the GRASP domain complex with a membrane, we studied the latter with NR, a technique that can determine the orientation of membrane-bound proteins of sufficient shape anisotropy within tight limits (34) and their localization along the membrane normal with Angstrom precision (24). The NR experiment involved the measurement of the as prepared and the protein-decorated stBLM, each under buffers of distinct isotopic compositions that contained $^{1}H_2O$ and $^{2}H_2O$ in different proportions. Because $^{1}H_2O$ and $^{2}H_2O$ differ in neutron scattering lengths, regions of the surface structure that contain water contribute differently to the scattering in isotopically distinct buffers, thereby facilitating the characterization of such regions within the sample. Neutron scattering is nondestructive, which allows all measurements to be conducted on the same sample area under identical conditions (19, 35). These measurements are then evaluated in reference to each other (24, 25) to obtain a unique, highly resolved model of the protein-membrane complex. Two complementing approaches to data modeling were

Downloaded from http://www.jbc.org/ by guest on August 29, 2018

employed. In both methods, the lipid membrane was described as continuous distributions of submolecular fragments (36). The contribution of the membrane-bound protein to the neutron scattering length density at the interface was modeled either as a sequence of spline functions ("model-free description") (21, 37) or by using the crystal structure of the GRASP domain (11) by rotating the structural model about two Euler angles and varying its distance from the membrane surface while optimizing the fit to the experimental data (24). Both models allowed for protein penetration into the bilayer, which was found to be small (<5 Å) in all cases.

NR was performed with myrG55 and G55, both at ~6 μM/liter protein, on DOPC stBLMs with 10 mol % Ni^{2+}-NTA-DGS. This protein concentration was sufficient to form a homogeneous protein layer at the interface in which the GRASP domain covered about 20% of the available area (Fig. 4*A*), necessary to resolve the structure of the interfacial protein with high confidence. Because the increase in Ni^{2+}-NTA-DGS content in the membrane led to an increase in bound protein area coverage, one might be concerned that molecular crowding at the interface biases the structural results. The following observations suggest that this is not the case. 1) Structural investigations with NR of other proteins at membrane surfaces, conducted at similar protein surface concentrations (21, 34, 38), showed clearly that protein organization depended on other factors (electrostatic interaction; ligand binding) than surface crowding. 2) A model that places proteins randomly on the surface (39) predicts mean nearest neighbor distances of 1.6 or 2.25 protein diameters, respectively, for area coverages of 20% (myrG55) or 10% (G55). Although dynamic protein-protein contacts are indeed likely on the fluid lipid bilayer of an stBLM (29), which may result in *cis* pairing due to PDZ interactions if protein orientation is not appropriately confined, unspecific interactions are rare as each membrane-bound protein still has ample space for lateral diffusion.

The obtained NR data sets from different isotopic buffers were fitted with neutron scattering length density profiles, which, in turn, are based on unique volume occupancy profiles of molecular components that were independent of isotopic compositions (36). Component volume occupancy (CVO) profiles thus determined in the model-free and atomistic approaches are shown in Fig. 4*A* (myrG55) and 4*B* (G55). The protein concentration at the membrane surface is larger by a factor >2 for the myristoylated protein. In both cases, the main features of the atomistic models are well within the confidence intervals of the free-form fits. The myristoylated GRASP domain most likely forms a unique protein-membrane complex, characterized by a specific orientation and penetration depth into the bilayer (Fig. 4, *C* and *D*). Because NR is insensitive to rotations of the sample about the membrane normal, the modeled reflectivities depend only on two of the three Euler angles, ϑ and φ, defined in the *inset* in Fig. 4*C* where $(\vartheta_0,\varphi_0) = (0°,0°)$ is defined in a Cartesian reference frame with the longest principle axis of the protein crystal structure aligned along the *z* axis (membrane normal) and the second longest principle axis aligned along the *x* axis. Monte-Carlo Markov chain data refinement provided the probabilities of protein orientations and penetration depths and yielded a narrow range of orientation angles centered on $(\vartheta,\varphi) = (26°,78°)$ (Fig. 4*C*). A region with arcs of $(\Delta\vartheta,\Delta\varphi) \sim (\pm 15°,\pm 20°)$ encloses the 95% (2σ) confidence intervals. This orientation places the myristoylated N terminus directly at the membrane surface and the C terminus into a position ~10 Å away, from where the His tag can reach the membrane surface via the decapeptide linker. The associated CVO profiles and oriented protein structure are shown in Fig. 4, *A* and *E*, respectively. The protein is peripherally associated with the membrane, penetrating the membrane's lipid headgroup region by <5 Å (Fig. 4*D*). The protein attains an upright orientation, with its longest principle axis, indicated by the *blue column* in Fig. 4*E*, tilted ~26° away from the surface normal, *z*. PDZ1 is close to the bilayer surface, and the center of mass of PDZ2 is further away by ~28 Å, such that the internal ligand on PDZ2 cannot bind to the groove of PDZ1 of neighboring molecules in the same bilayer. The axes of the internal ligand and its target groove (yellow cylinders) are almost parallel, with an angular mismatch of ~5°. Both point down toward the membrane surface (*x-y* plane, shown in *blue* in Fig. 4*E*) at shallow angles. Colored beads indicate locations of the N and C termini determined. Steered MD simulations in which only amino acid residues not resolved in the crystal structure as well as the added C-terminal decapeptide and His_6 tag were allowed to vary conformationally were used to bring both termini to the membrane interface. Overall, this model of the protein/membrane complex resembles the protein organization schematically shown in Fig. 1*B* and is distinct from our previous depiction (11) resembling that of Fig. 1*A*.

In contrast to myrG55, a unique organization of the nonmyristoylated G55 on the membrane cannot be distinguished from the NR data with confidence because multiple orientations lead to similar NR spectra. However, G55 shows a significantly smaller extension from the membrane surface into the bulk than myrG55 (~40 Å *versus* ~60 Å, compare Fig. 4, *A* and *B*). The CVO profiles for the various orientations that are compatible with the NR results are consistent with arrangements in which the GRASP domain rests on its side (ϑ >45°), with both PDZ domains near the membrane surface, as schematically shown in Fig. 1*C*. Because these ranges of orientational states give rise to similar CVO profiles, a particular protein orientation cannot be determined, nor can it be excluded that multiple orientational states, and therefore distinct structures of the protein/membrane complex, coexist. An alternate arrangement with a more upright orientation is also consistent with the NR results, but the protein would have to penetrate the membrane significantly (Fig. 4*F*). Unless further work unexpectedly indicates that GRASP penetrates the membrane, this orientation seems unlikely. A more complete account of the NR results and their evaluation is provided in supplemental Figs. S1–S13 and supplemental Tables S1–S4.

DISCUSSION

Membrane tethering that involves *trans* complex formation is widespread and important in cell biology, but an understanding of how it occurs in the face of competing *cis* pairing is incomplete. We found that the purified GRASP domain is sufficient to mediate membrane tethering. This tethering occurred via GRASP domain self-interactions, as GRASP

Downloaded from http://www.jbc.org/ by guest on August 29, 2018

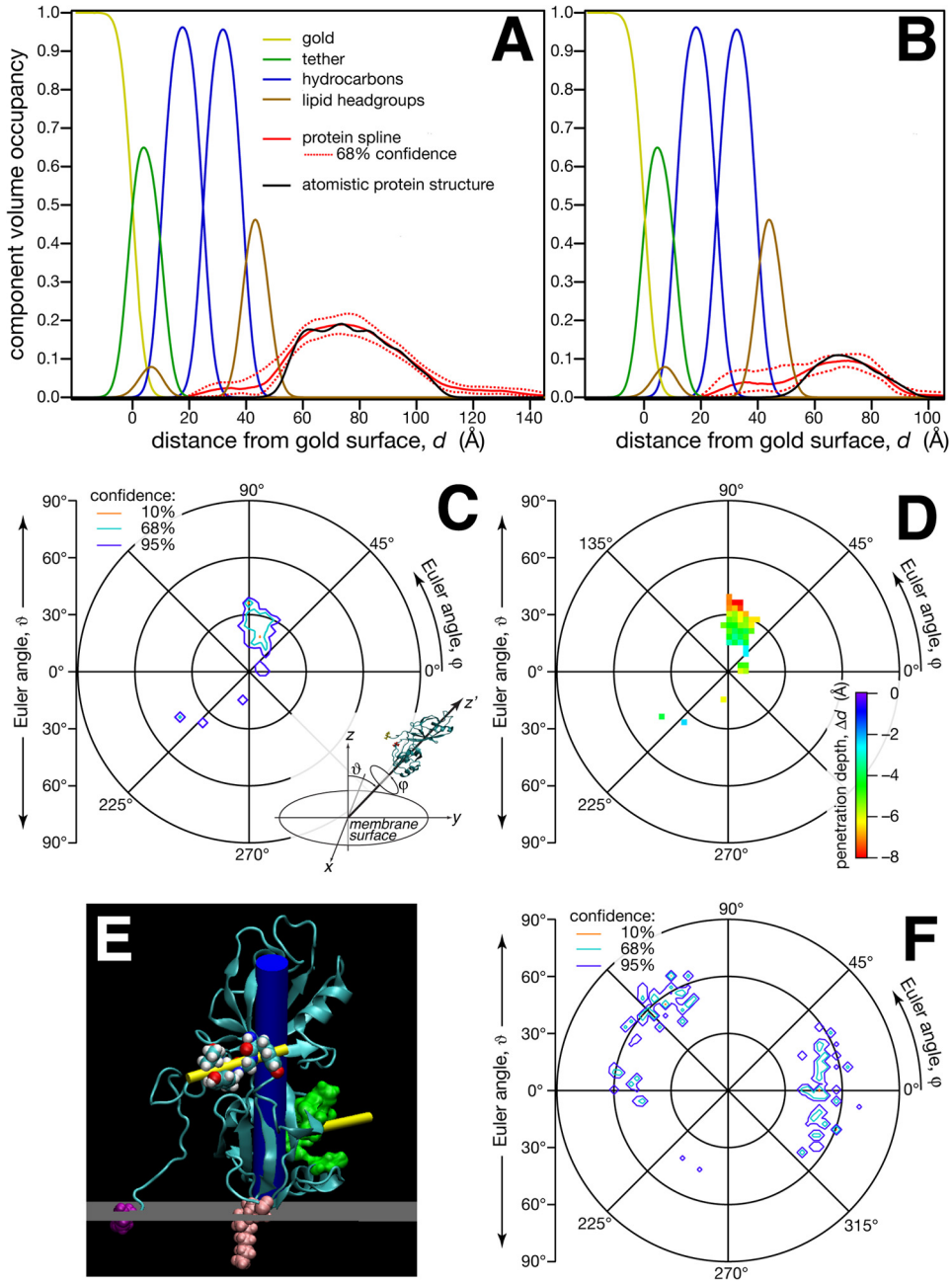

FIGURE 4. **Complex structure of the GRASP55 GRASP domain with a membrane.** *A* and *B*, fractional CVO profiles of stBLMs composed of DOPC and Ni^{2+}-NTA-DGS (9:1) on HC18/β-mercaptoethanol (1:3) with 6.5 μmol/liter myrG55 (*A*) and 6 μmol/liter G55 (*B*). CVO profiles of the substrate (terminal gold film), oligo(ethylene oxide) tether, lipid bilayer components, and protein, indicated in the legend in *A*, are decomposed from multiple NR measurements. Protein CVO profiles determined from spline fits (*red lines*) and from atomistic models (*black dashed lines*) are shown in the same graphs for comparison. Lipid bilayer CVO profiles shown are those determined from the free-form fits and are very similar in the atomistic models. *Dashed red lines* indicate 68% confidence intervals for the free-form protein CVO profiles. *C*, probability distribution, determined from Monte Carlo data resampling (25), of myrG55 orientations (ϑ,φ) with respect to the bilayer normal. Only the half-sphere $0 \leq \vartheta \leq 90°$ is shown. The best fit is observed at $(\vartheta,\varphi) = (26°,78°)$. The *inset* shows the definition of the Euler angles ϑ and φ. *D*, penetration depths of myrG55 into the bilayer at the orientations shown in *panel C*. The membrane surface is defined as the half-point in the decay of the lipid headgroup CVO toward bulk buffer (*brown traces* in *panels A* and *B* at $d \sim 50$ Å). *E*, orientation of myrG55 on the bilayer that corresponds to the best fit, $(\vartheta,\varphi) = (26°,78°)$, in the probability distribution of *panel C*. The long principal axis of the GRASP55 GRASP domain, $\vartheta_0 = 0°$, is shown as a *blue column*. The internal ligand on the PDZ2 domain is shown in *volume-filling representation*, and the PDZ1 binding groove is shown as a *green surface*. The orientations of the PDZ2 ligand and a putative ligand bound to the PDZ1 groove, indicated as *yellow cylinders*, are roughly collinear. Approximate positions of the C- and N-terminal membrane binding sites, *i.e.* the Ni^{2+}-ligated His tag and the myristoyl group, are shown in *purple* and *maroon*, respectively. *F*, probability distribution of G55 orientations (ϑ,φ) with respect to the bilayer normal on the half-sphere $0 \leq \vartheta \leq 90°$.

needed to be present on both membranes and blocking mutations at the interaction interface inhibited tethering. In our assay, membrane anchoring of the GRASP domain was achieved via the N-terminal myristic acid and binding of a C-terminal His tag to Ni^{2+}-conjugated lipids. Although the latter contact alone resulted in stable anchoring of the protein on each membrane surface, efficient tethering required both anchor points. Our structural studies showed that the dually anchored GRASP domain is complexed with the membrane in a unique, upright orientation that is likely compatible with the

Downloaded from http://www.jbc.org/ by guest on August 29, 2018

formation of interdigitated multimeric tethering complexes (Fig. 1*B*). In the absence of myristoylation, such a unique protein orientation could not be established, and the GRASP domain-membrane complex structure is more likely consistent with that depicted in Fig. 1*C*, which allows the formation of unproductive *cis* dimers.

As with the GRASP proteins, myristoylated proteins often depend on additional interactions for stable membrane association at their correct cellular localization. Therefore, *N*-myristoylation creates a second membrane attachment point, raising the possibility that a general purpose of *N*-myristoylation is to restrict protein orientation on the membrane, which could be beneficial to many protein functions. In the case of the GRASP domain, we show here that dual anchoring establishes an orientation that appears incompatible with homotypic interactions in *cis*. For membrane proteins that interact with the cytoskeleton, a similar mechanism could favor selective binding based on filament orientations. For protein-protein interactions within the plane of the membrane or for soluble components assembling on membrane proteins, myristoylation could control the final geometry of the complex.

Although protein orientation is likely a key determinant in many tethering reactions including cadherin-mediated cell-cell adhesion (1), this mechanism is ill-suited for flexible or unstructured binding partners. For example, the SNARE family of membrane-tethering/fusion proteins readily undergoes interactions in *cis*, forming stable complexes. ATP hydrolysis by the NSF ATPase is required to disassemble these complexes, enabling the SNARE proteins to participate in *trans* interactions. Thus, there exist at least two distinct modes of controlling *trans* interactions. Although an active mechanism, such as NSF, is needed to disassemble stable *cis* complexes of SNARES, membrane orientation may serve for well structured proteins.

Orientation-dependent binding could also impact the eventual dissociation of GRASP tethering complexes. This is because GRASP-mediated tethering precedes membrane fusion and the membrane rearrangement that occurs upon fusion transforms GRASP complexes from *trans* to *cis*. Our results here suggest that membrane-associated GRASP complexes in *cis* could only persist if the surrounding membrane forms a highly strained, *i.e.* high energy (40), configuration. Assuming that the GRASP membrane association *in vivo* is sufficiently strong, the relatively weak PDZ-ligand interaction (16) may provide a predetermined breaking point that releases once membrane fusion is completed. Thus, membrane fusion may provide the energy to dissociate GRASP *trans* complexes. This would constitute a novel type of regulation in which protein-protein interaction is controlled by membrane dynamics.

It is also conceivable that by providing a second membrane contact point, *N*-myristoylation confers a conformational change to the GRASP domain that affects its propensity for self-interaction. As peripheral membrane proteins, GRASP proteins are present in the cytosol, at least in small concentrations. Thus, both the membrane association of preformed soluble dimers and the binding of a soluble monomer to a membrane-associated monomer could render membrane tethering inefficient. Therefore, a reasonable hypothesis is that membrane binding imparts a conformational change, which activates the GRASP domains for self-interaction. Indeed, the purified GRASP55 GRASP domain self-interacts only weakly in solution (33).

The tethering assay described here allows manipulation of its core components, including lipid composition, liposome size, surface density of the proteins, and buffer composition. Although not physiological, the membrane anchoring of the GRASP domain using the His tag is a versatile aspect of the assay. Myristoylated GRASPs are recruited to Golgi membranes by binding golgins (14). Thus, further efforts to better recapitulate the biological tethering complex will be directed toward anchoring a His-tagged golgin such that the GRASP-binding domain of the golgin will recruit the myristoylated GRASP.

In conclusion, this study reveals an elegant structure-based biological mechanism that promotes homotypic protein-protein interactions in *trans* in which myristoylation stabilizes protein membrane orientation, thereby preventing interactions in *cis*. The work also shows that the GRASP domain is sufficient to mediate membrane tethering. An important area of further study concerns how additional cellular factors contribute to GRASP-mediated tethering. It will also be exciting to investigate whether myristoylation restricts the orientation of other proteins and to determine the ways in which orientation participates in the diverse functions of membrane proteins.

Acknowledgments—We thank Dr. D. J. Vanderah for the HC18 compound and Dr. D. J. McGillivray for help with some neutron measurements. Parts of this research were performed at the NIST Centers for Neutron Research and Nanoscale Science and Technology. This study utilized computational capabilities through the Extreme Science and Engineering Discovery Environment (XSEDE) supported by the NSF (OCI-0503697) with computations performed at the National Institute for Computational Sciences (NICS).

REFERENCES

1. Brasch, J., Harrison, O. J., Honig, B., and Shapiro, L. (2012) Thinking outside the cell: how cadherins drive adhesion. *Trends Cell Biol.* **22,** 299–310
2. Berkhout, B., Eggink, D., and Sanders, R. W. (2012) Is there a future for antiviral fusion inhibitors? *Curr. Opin. Virol.* **2,** 50–59
3. Waters, M. G., and Pfeffer, S. R. (1999) Membrane tethering in intracellular transport. *Curr. Opin. Cell Biol.* **11,** 453–459
4. Voeltz, G. K., and Prinz, W. A. (2007) Sheets, ribbons and tubules – how organelles get their shape. *Nat. Rev. Mol. Cell Biol.* **8,** 258–264
5. Puthenveedu, M. A., Bachert, C., Puri, S., Lanni, F., and Linstedt, A. D. (2006) GM130 and GRASP65-dependent lateral cisternal fusion allows uniform Golgi-enzyme distribution. *Nat. Cell Biol.* **8,** 238–248
6. Feinstein, T. N., and Linstedt, A. D. (2008) GRASP55 regulates Golgi ribbon formation. *Mol. Biol. Cell* **19,** 2696–2707
7. Barr, F. A., Puype, M., Vandekerckhove, J., and Warren, G. (1997) GRASP65, a protein involved in the stacking of Golgi cisternae. *Cell* **91,** 253–262
8. Shorter, J., Watson, R., Giannakou, M. E., Clarke, M., Warren, G., and Barr, F. A. (1999) GRASP55, a second mammalian GRASP protein involved in the stacking of Golgi cisternae in a cell-free system. *EMBO J.* **18,** 4949–4960
9. Xiang, Y., and Wang, Y. (2010) GRASP55 and GRASP65 play complementary and essential roles in Golgi cisternal stacking. *J. Cell Biol.* **188,** 237–251
10. Jarvela, T., and Linstedt, A. D. (2014) Isoform-specific tethering links the

Downloaded from http://www.jbc.org/ by guest on August 29, 2018

Golgi ribbon to maintain compartmentalization. *Mol. Biol. Cell* **25,** 133–144
11. Truschel, S. T., Sengupta, D., Foote, A., Heroux, A., Macbeth, M. R., and Linstedt, A. D. (2011) Structure of the membrane-tethering GRASP domain reveals a unique PDZ ligand interaction that mediates Golgi biogenesis. *J. Biol. Chem.* **286,** 20125–20129
12. Sengupta, D., Truschel, S., Bachert, C., and Linstedt, A. D. (2009) Organelle tethering by a homotypic PDZ interaction underlies formation of the Golgi membrane network. *J. Cell Biol.* **186,** 41–55
13. Barr, F. A., Nakamura, N., and Warren, G. (1998) Mapping the interaction between GRASP65 and GM130, components of a protein complex involved in the stacking of Golgi cisternae. *EMBO J.* **17,** 3258–3268
14. Short, B., Preisinger, C., Körner, R., Kopajtich, R., Byron, O., and Barr, F. A. (2001) A GRASP55-rab2 effector complex linking Golgi structure to membrane traffic. *J. Cell Biol.* **155,** 877–883
15. Bachert, C., and Linstedt, A. D. (2010) Dual anchoring of the GRASP membrane tether promotes *trans* pairing. *J. Biol. Chem.* **285,** 16294–16301
16. Nourry, C., Grant, S. G., and Borg, J. P. (2003) PDZ domain proteins: plug and play! *Sci. STKE* **2003,** RE7
17. Budvytyte, R., Valincius, G., Niaura, G., Voiciuk, V., Mickevicius, M., Chapman, H., Goh, H. Z., Shekhar, P., Heinrich, F., Shenoy, S., Lösche, M., and Vanderah, D. J. (2013) Structure and properties of tethered bilayer lipid membranes with unsaturated anchor molecules. *Langmuir* **29,** 8645–8656
18. Sengupta, D., and Linstedt, A. D. (2010) Mitotic inhibition of GRASP65 organelle tethering involves polo-like kinase 1 (PLK1) phosphorylation proximate to an internal PDZ ligand. *J. Biol. Chem.* **285,** 39994–40003
19. McGillivray, D. J., Valincius, G., Vanderah, D. J., Febo-Ayala, W., Woodward, J. T., Heinrich, F., Kasianowicz, J. J., and Lösche, M. (2007) Molecular-scale structural and functional characterization of sparsely tethered bilayer lipid membranes. *Biointerphases* **2,** 21–33
20. Valincius, G., McGillivray, D. J., Febo-Ayala, W., Vanderah, D. J., Kasianowicz, J. J., and Lösche, M. (2006) Enzyme activity to augment the characterization of tethered bilayer membranes. *J. Phys. Chem. B* **110,** 10213–10216
21. Shenoy, S., Shekhar, P., Heinrich, F., Daou, M.-C., Gericke, A., Ross, A. H., and Lösche, M. (2012) Membrane association of the PTEN tumor suppressor: Molecular details of the protein-membrane complex from SPR binding studies and neutron reflection. *PLoS ONE* **7,** e32591
22. Cornell, B. A., Braach-Maksvytis, V. L. B., King, L. G., Osman, P. D. J., Raguse, B., Wieczorek, L., and Pace, R. J. (1997) A biosensor that uses ion-channel switches. *Nature* **387,** 580–583
23. Kirby, B. J., Kienzle, P. A., Maranville, B. B., Berk, N. F., Krycka, J., Heinrich, F., and Majkrzak, C. F. (2012) Phase-sensitive specular neutron reflectometry for imaging the nanometer scale composition depth profile of thin-film materials. *Curr. Opin. Colloid Interf. Sci.* **17,** 44–53
24. McGillivray, D. J., Valincius, G., Heinrich, F., Robertson, J. W. F., Vanderah, D. J., Febo-Ayala, W., Ignatjev, I., Lösche, M., and Kasianowicz, J. J. (2009) Structure of functional *Staphylococcus aureus* α-hemolysin channels in tethered bilayer lipid membranes. *Biophys. J.* **96,** 1547–1553
25. Heinrich, F., Ng, T., Vanderah, D. J., Shekhar, P., Mihailescu, M., Nanda, H., and Lösche, M. (2009) A new lipid anchor for sparsely tethered bilayer lipid membranes. *Langmuir* **25,** 4219–4229
26. Phillips, J. C., Braun, R., Wang, W., Gumbart, J., Tajkhorshid, E., Villa, E., Chipot, C., Skeel, R. D., Kalé, L., and Schulten, K. (2005) Scalable molecular dynamics with NAMD. *J. Comput. Chem.* **26,** 1781–1802
27. MacKerell, A. D., Bashford, D., Bellott, M., Dunbrack, R. L., Evanseck, J. D., Field, M. J., Fischer, S., Gao, J., Guo, H., Ha, S., Joseph-McCarthy, D., Kuchnir, L., Kuczera, K., Lau, F. T. K., Mattos, C., Michnick, S., Ngo, T., Nguyen, D., Prodhom, B., Reiher, W. E., Roux, B., Schlenkrich, M., Smith, J. C., Stote, R., Straub, J., Watanabe, M., Wiorkiewicz-Kuczera, J., Yin, D., and Karplus, M. (1998) All-atom empirical potential for molecular modeling and dynamics studies of proteins. *J. Phys. Chem. B* **102,** 3586–3616
28. Klauda, J. B., Venable, R. M., Freites, J. A., O'Connor, J. W., Tobias, D. J., Mondragon-Ramirez, C., Vorobyov, I., MacKerell, A. D., Jr., and Pastor, R. W. (2010) Update of the CHARMM all-atom additive force field for lipids: Validation on six lipid types. *J. Phys. Chem. B* **114,** 7830–7843
29. Shenoy, S., Moldovan, R., Fitzpatrick, J., Vanderah, D. J., Deserno, M., and Lösche, M. (2010) In-plane homogeneity and lipid dynamics in tethered bilayer lipid membranes (tBLMs). *Soft Matter* **2010,** 1263–1274
30. Gizeli, E., and Glad, J. (2004) Single-step formation of a biorecognition layer for assaying histidine-tagged proteins. *Anal. Chem.* **76,** 3995–4001
31. Nye, J. A., and Groves, J. T. (2008) Kinetic control of histidine-tagged protein surface density on supported lipid bilayers. *Langmuir* **24,** 4145–4149
32. Peitzsch, R. M., and McLaughlin, S. (1993) Binding of acylated peptides and fatty acids to phospholipid vesicles: pertinence to myristoylated proteins. *Biochemistry* **32,** 10436–10443
33. Truschel, S. T., Zhang, M., Bachert, C., Macbeth, M. R., and Linstedt, A. D. (2012) Allosteric regulation of GRASP protein-dependent Golgi membrane tethering by mitotic phosphorylation. *J. Biol. Chem.* **287,** 19870–19875
34. Nanda, H., Datta, S. A. K., Heinrich, F., Lösche, M., Rein, A., Krueger, S., and Curtis, J. E. (2010) Electrostatic interactions and binding orientation of HIV-1 matrix, studied by neutron reflectivity. *Biophys. J.* **99,** 2516–2524
35. Dura, J. A., Pierce, D. J., Majkrzak, C. F., Maliszewskyj, N. C., McGillivray, D. J., Lösche, M., O'Donovan, K. V., Mihailescu, M., Perez-Salas, U., Worcester, D. L., and White, S. H. (2006) AND/R: A neutron diffractometer/reflectometer for investigation of thin films and multilayers for the life sciences. *Rev. Sci. Instrum.* **77,** 74301–7430111
36. Shekhar, P., Nanda, H., Lösche, M., and Heinrich, F. (2011) Continuous distribution model for the investigation of complex molecular architectures near interfaces with scattering techniques. *J. Appl. Phys.* **110,** 102216–10221612
37. Pfefferkorn, C. M., Heinrich, F., Sodt, A. J., Maltsev, A. S., Pastor, R. W., and Lee, J. C. (2012) Depth of α-synuclein in a bilayer determined by fluorescence, neutron reflectometry, and computation. *Biophys. J.* **102,** 613–621
38. Datta, S. A. K., Heinrich, F., Raghunandan, S., Krueger, S., Curtis, J. E., Rein, A., and Nanda, H. (2011) HIV-1 Gag extension: Conformational changes require simultaneous interaction with membrane and nucleic acid. *J. Mol. Biol.* **406,** 205–214
39. Torquato, S. (1995) Mean nearest-neighbor distance in random packings of hard D-dimensional spheres. *Phys. Rev. Lett.* **74,** 2156–2159
40. Helfrich, W. (1973) Elastic properties of lipid bilayers: theory and possible experiments. *Z. Naturforsch C.* **28,** 693–703

Downloaded from http://www.jbc.org/ by guest on August 29, 2018

version: Jan 31, 2014

Supplemental Data:

Myristoylation Restricts Orientation of the GRASP domain on Membranes and Promotes Membrane Tethering

Neutron Reflectometry: Original Data, Model Fits and Best-Fit Parameters

Haw Zan Goh, Hirsh Nanda, Frank Heinrich, Collin Bachert, Adam Linstedt, and Mathias Lösche

1. Unmyristoylated full-length G55: GRASP55(1–208)-His_6 (April 2013)
NR spectra and best-fit model reflectivities (model parameters: Table S1)

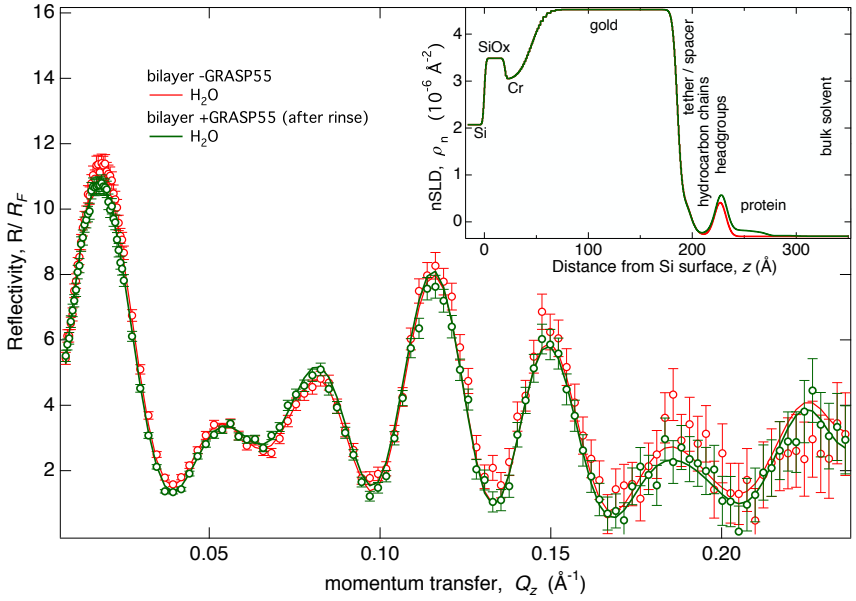

Figure S1: Fresnel-normalized NR and best-fit reflectivities (inset: nSLD profiles) for G55 in H_2O-based buffer.

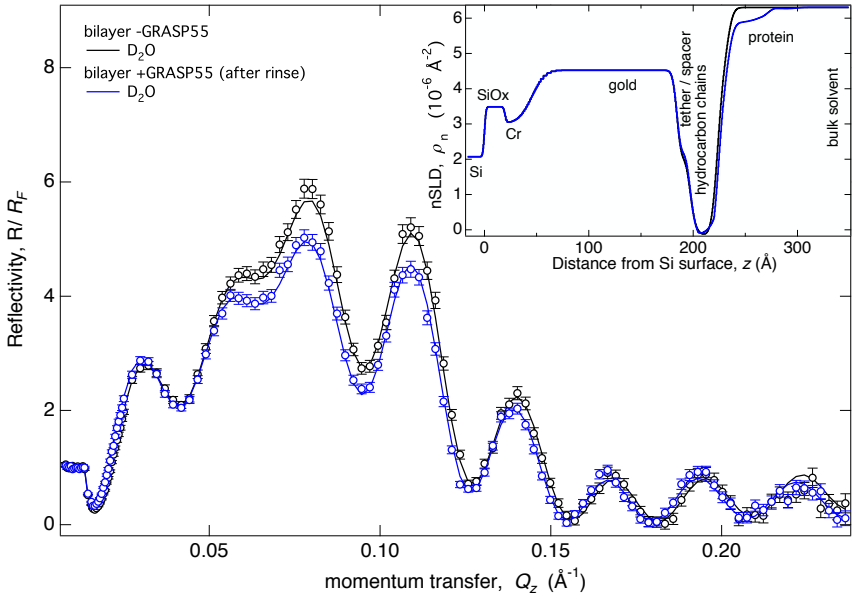

Figure S2: Fresnel-normalized NR and best-fit reflectivities (inset: nSLD profiles) for G55 in D_2O-based buffer.

Best-fit parameters

Parameter	Bilayer without G55	Bilayer + G55
Substrate		
Silicon oxide	Thickness: 18.5 ± 3.7 Å, ρ: 3.46 ± 0.14 10^{-6} Å^{-2}	
Chromium	Thickness: 27.6 ± 3.4 Å, ρ: 3.04 ± 0.02 10^{-6} Å^{-2}	
Gold	Thickness: 139.1 ± 0.8 Å, ρ: 4.45 ± 0.03 10^{-6} Å^{-2}	
Substrate roughness (sigma) / Å	2.6 ± 0.9	
Cr / Au roughness	9.5 ± 0.8	
Lipid bilayer		
Thickness tether / Å	10.7 ± 0.4	
Molar fraction of tether in inner lipid leaflet	0.56 ± 0.42	
Number of βME molecules per tether	2.6 ± 1.7	
Thickness inner hydrocarbon chains / Å	15.0 ± 0.6	Change: +1.8 ± 0.5
Thickness outer hydrocarbon chains / Å	14.0 ± 0.5	
Completeness of lipid bilayer	0.99 ± 0.03	0.98 ± 0.02
Bilayer roughness (sigma) / Å	4.6 ± 0.7	
Protein		
Penetration depth of protein into lipid bilayer (measured from the headgroup - bulk solvent interface) / Å		6.8 ± 7.9
Fraction of exchangeable protons that exchange		0.79 ± 0.20
Amount of protein at the membrane / Å^3 / Å^2 surface area		After second rinse: 3.1 ± 0.4 [≡ 39 ± 5 ng/cm^2]
Fraction of protein remaining at the interface after second rinse		0.83 ± 0.21
Best-fit orientation and penetration		(ϑ,φ) = (52°,353°) penetration: 7.5 Å
Global		
Best-fit χ^2	1.01	

Table S1: G55 protein on stBLM – median fit parameters and 68% confidence intervals.

Orientation distributions consistent with NR data

Orientation fit results (Fig. S3: full 4π space) using the crystal structure (3RLE) of the GRASP55 GRASP domain completed with the residues not included in the crystal structure. After adding the residues, a short solution MD simulation was performed to obtain a realistic conformation of the added residues. 20 frames from this simulation were averaged for use in the orientation fit. No unique orientation can be identified. Median values of fit parameters and confidence intervals are provided in Table S1. Orientation maps of penetration depth and χ2 values are provided in Figs. S4 and S5.

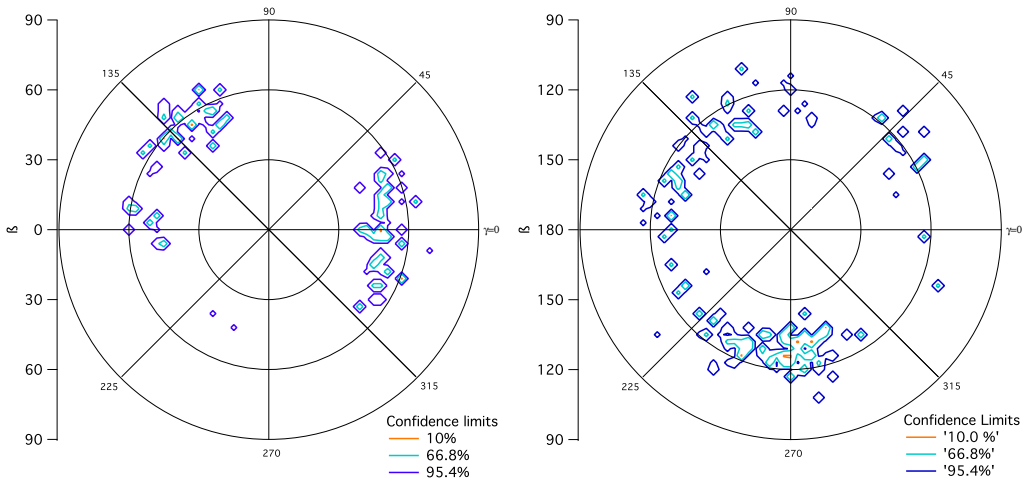

Figure S3: MCMC orientation analysis for unmyristoylated G55 using the full-length GRASP55 structure. The (0,0) orientation aligns the first principal axis of the protein with the membrane normal.

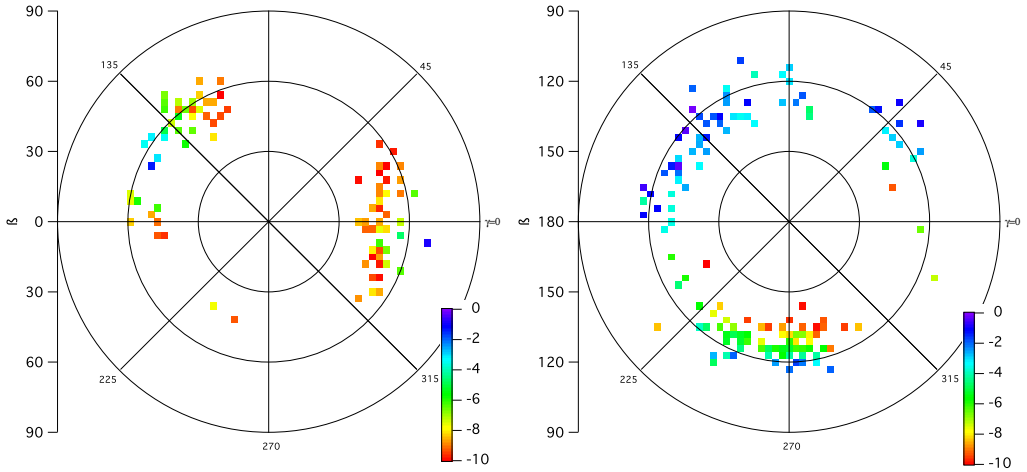

Figure S4: MCMC orientation maps of the G55 penetration depth into the lipid bilayer.

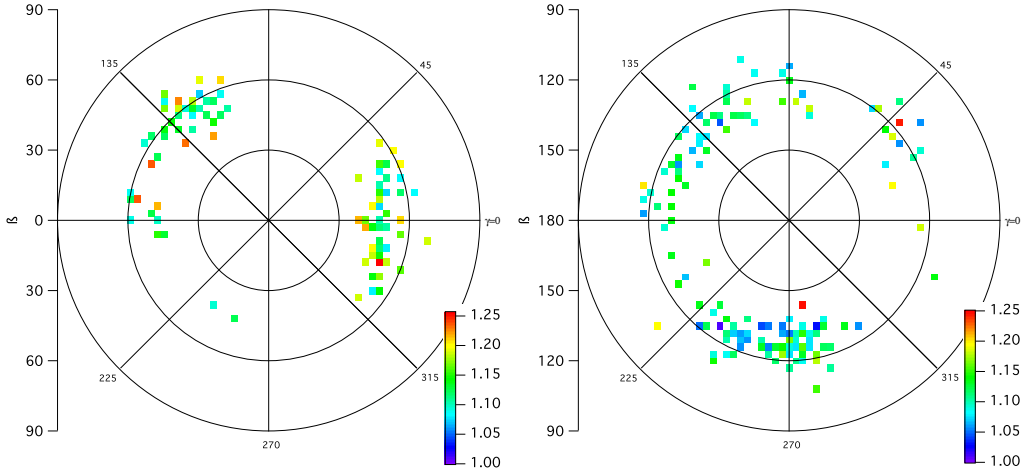

Figure S5: MCMC-derived maps of the best-fit χ2 values for the G55 orientations shown in Fig. S3.

2. Myristoylated full-length G55: myrGRASP55(1–208)-His$_6$ (October 2012)

NR spectra and best-fit model reflectivities (model parameters: Table S2)

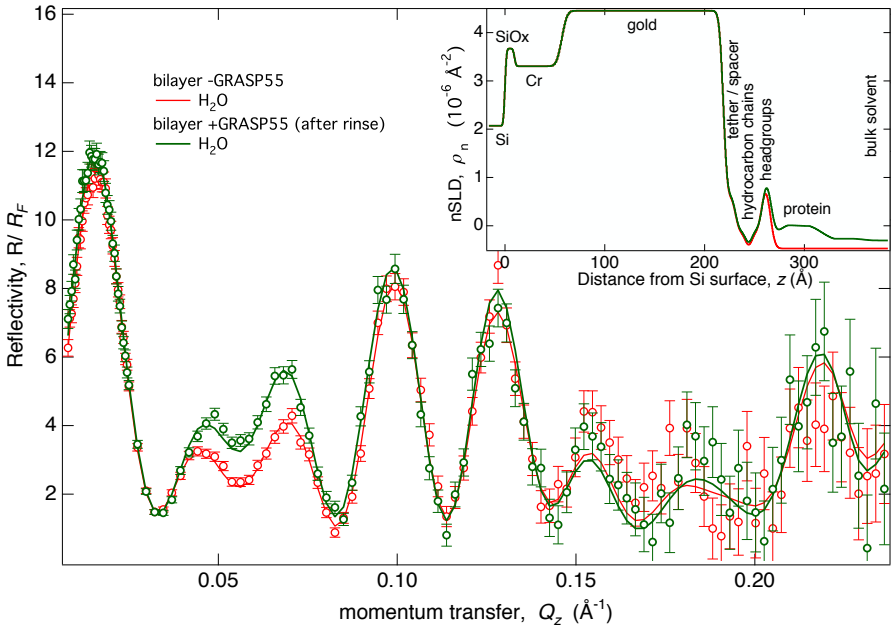

Figure S6: Fresnel-normalized NR and best-fit reflectivities (inset: nSLD profiles) for myrG55 in H_2O-based buffer.

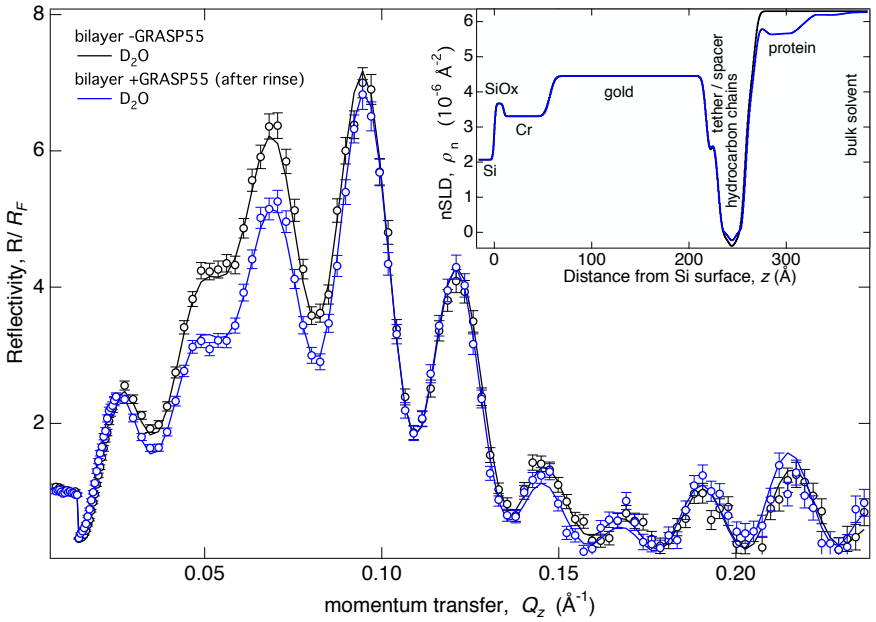

Figure S7: Fresnel-normalized NR and best-fit reflectivities (inset: nSLD profiles) for myrG55 in D_2O-based buffer.

Data evaluation

The data was analyzed in two ways. First, a spline fit was carried out in which no assumptions are made about the protein CVO. Second, a fit of the neutron data was carried out that assumes that the overall protein shape is according to the 3RLE PDB file (in an unknown orientation with respect to the bilayer). In this second fit, the PDB structure is rotated near the membrane and the distance of the

protein to the membrane is simultaneously adjusted. Thus, a binding orientation of the protein is determined. In a third step, the amino acid residues that are not included in 3RLE were added to the PDB file using molecular modeling and the membrane orientation/distance of that protein determined.

Spline Fit

The NR data was fit using a continuous distribution model for the lipid bilayer and a monotonic Hermite spline for the protein. The distance between the control points of the spline is 15 Å on average. Each control point can deviate from its center position by ± 5 Å. The protein profile is constrained to be single-peaked. Median parameters and confidence intervals are shown in Table S2.

Parameter	**Bilayer without myrG55**	**Bilayer + myrG55**
Substrate		
Silicon oxide	Thickness: 10.3 ± 3.4 Å, ρ: 3.62 ± 0.13 10^{-6} Å^{-2}	
Chromium	Thickness: 46.9 ± 3.2 Å, ρ: 3.29 ± 0.02 10^{-6} Å^{-2}	
Gold	Thickness: 161.5 ± 0.3 Å, ρ: 4.43 ± 0.03 10^{-6} Å^{-2}	
Substrate roughness / Å	3.0 ± 0.4	
Gold/chromium roughness / Å	9.9 ± 0.2	
Lipid bilayer		
Thickness tether / Å	11.0 ± 0.2	
Molar fraction of tether in inner lipid leaflet	0.44 ± 0.20	
Number of βME molecules per tether	4.1 ± 1.2	
Thickness inner hydrocarbon chains / Å	14.5 ± 0.3	Change: +0.8 ± 0.2
Thickness outer hydrocarbon chains / Å	14.6 ± 0.4	
Completeness of lipid bilayer	1.00 ± 0.01	0.98 ± 0.01
Bilayer roughness	2.8 ± 0.3	
Protein		
Fraction of exchangeable protons that exchange		0.87 ± 0.20
Fraction of protein remaining at the interface after second rinse		0.91 ± 0.08
Total amount of protein at interface / Å^3 / Å^2 surface area		After second rinse: 10.0 ± 0.9 [≡ 127 ± 11 ng/cm^2]
Global		
Best-fit χ^2	1.03	

Table S2: Full-length myrG55 protein on stBLM – median fit parameters and 68% confidence intervals for spline fit.

Orientation Fits

(a) Full-length GRASP55, random orientation of added peptides

The orientation fit here uses the 3RLE protein coordinate set completed with the missing residues (including the synthetic decapeptide and His-tag). After adding the residues, a short solution MD simulation was performed to obtain a realistic conformation. 20 frames from this simulation were averaged for use in the orientation fit. Median parameters and confidence intervals are shown in Table S3.

Parameter	Bilayer without myrG55	Bilayer + myrG55
Substrate		
Silicon oxide	Thickness: 19.5 ± 2.9 Å, ρ: 3.43 ± 0.05 10^{-6} Å^{-2}	
Chromium	Thickness: 38.0 ± 2.9 Å, ρ: 3.22 ± 0.02 10^{-6} Å^{-2}	
Gold	Thickness: 162.4 ± 0.4 Å, ρ: 4.35 ± 0.02 10^{-6} Å^{-2}	
Substrate roughness (sigma) / Å	2.6 ± 0.6	
Cr / Au roughness	14.8±0.4	
Lipid bilayer		
Thickness tether / Å	10.9 ± 0.2	
Molar fraction of tether in inner lipid leaflet	0.60 ± 0.29	
Number of βME molecules per tether	3.0 ± 1.2	
Thickness inner hydrocarbon chains / Å	14.8 ± 0.3	Change: +0.8 ± 0.3
Thickness outer hydrocarbon chains / Å	14.5 ± 0.4	
Completeness of lipid bilayer	1.00 ± 0.01	0.98 ± 0.01
Bilayer roughness (sigma) / Å	2.2 ± 0.2	
Protein		
Penetration depth of protein into lipid bilayer (measured from the headgroup - bulk solvent interface) / Å		4.9 ± 1.6
Fraction of exchangeable protons that exchange		0.67 ± 0.10
Fraction of protein remaining at the interface after second rinse		0.86 ± 0.08
Amount of protein at the membrane / Å^3 / Å^2 surface area		After second rinse: 8.0 ± 0.5 [≡ 102 ± 6 ng/cm^2]
Best-fit orientation and penetration		(ϑ,φ) = (26°,78°) penetration: 5.3 Å
Global		
Best-fit χ^2	1.11	

Table S3: Full-length myrG55 protein on stBLM – median fit parameters and 68% confidence intervals for orientation fit.

Orientation fit results for myrG55 (Fig. S8: full 4π space) using the crystal structure (3RLE) of the GRASP55 GRASP domain completed with the peptide residues not included in the crystal structure. After adding the residues, a short solution MD simulation was performed to obtain a realistic conformation of the added residues. 20 frames from this simulation were averaged for use in the orientation fit. A unique orientation of the myrG55 protein emerges from this analysis near (ϑ,φ) = (26°,78°). While intensity is also observed near the antipode (ϑ,φ) ≈ (150°,120°) and, to a lesser extent near (ϑ,φ) ≈ (140°,225°), these orientations can be ruled out because the N- and C-termini do not reach the membrane surface in that orientation. Median values of fit parameters and confidence intervals are provided in Table S3. Orientation maps of penetration depth and χ2 values are provided in Figs. S9 and S10.

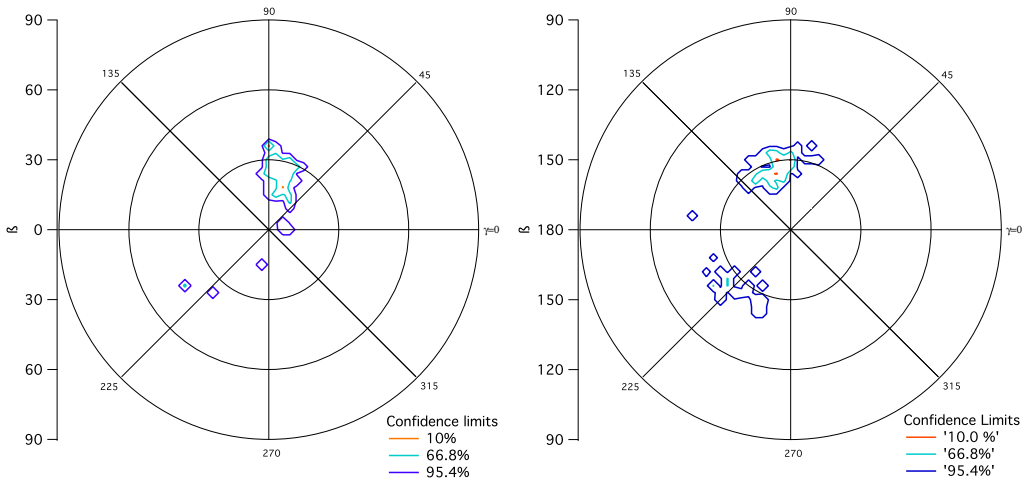

Figure S8: MCMC orientation analysis for myrG55 using the full-length GRASP55 structure with added peptide (not optimized for membrane association of the N and C termini).

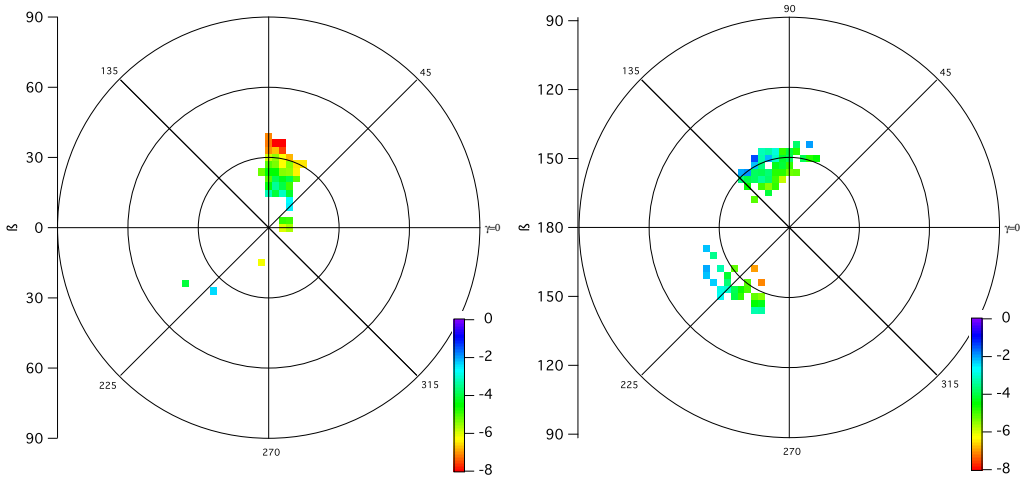

Figure S9: MCMC orientation maps of the myrG55 penetration depth into the lipid bilayer.

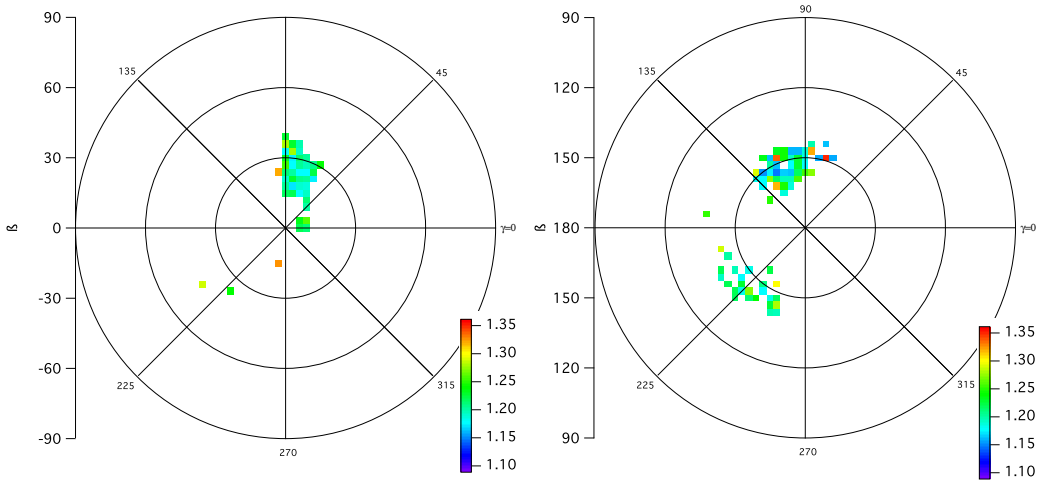

Figure S10: MCMC-derived maps of the best-fit χ2 values for the G55 orientations shown in Fig. S8.

(b) Full-length GRASP55 with C- and N-termini pulled down towards membrane

In a final step of model refinement, we modified the full-length myrG55 structure, as defined in the last section, by modifying the organization of the C- and N-termini in a steered MD simulation such that they extended to the membrane plane identified as described above. The orientation fit was then repeated with this modified full-length myrG55 structure. No significant changes between this and the previous optimized fit were observed. The fit quality is marginally better compared to the previous results, see Table S4.

Parameter	**Bilayer without G55**	**Bilayer + G55**
Substrate		
Silicon oxide	Thickness: 19.6 ± 2.7 Å, ρ: 3.43 ± 0.05 10^{-6} Å^{-2}	
Chromium	Thickness: 37.7 ± 2.4 Å, ρ: 3.22 ± 0.02 10^{-6} Å^{-2}	
Gold	Thickness: 162.5 ± 0.4 Å, ρ: 4.34 ± 0.02 10^{-6} Å^{-2}	
Substrate roughness (sigma) / Å	2.7 ± 0.6	
Cr / Au roughness	14.8±0.4	
Lipid bilayer		
Thickness tether / Å	10.9 ± 0.2	
Molar fraction of tether in inner lipid leaflet	0.59 ± 0.34	
Number of βME molecules per tether	3.0 ± 1.4	
Thickness inner hydrocarbon chains / Å	14.9 ± 0.4	Change: +0.8 ± 0.2
Thickness outer hydrocarbon chains / Å	14.5 ± 0.5	
Completeness of lipid bilayer	1.00 ± 0.01	0.97 ± 0.01
Bilayer roughness (sigma) / Å	2.2 ± 0.2	
Protein		
Penetration depth of protein into lipid bilayer (measured from the headgroup - bulk solvent interface) / Å		4.6 ± 1.3
Fraction of exchangeable protons that exchange		0.72 ± 0.13
Fraction of protein remaining at the interface after second rinse		0.94 ± 0.04
Amount of protein at the membrane / Å^3 / Å^2 surface area		After second rinse: 7.8 ± 0.5 [≡ 99 ± 6 ng/cm^2]
Best-fit orientation and penetration		$(\vartheta,\varphi) = (25^o,80^o)$ penetration: 3.8 Å
Global		
Best-fit χ^2	1.07	

Table S4: Full-length myrG55 protein (optimized peptide additions) on stBLM – median fit parameters and 68% confidence intervals for orientation fit.

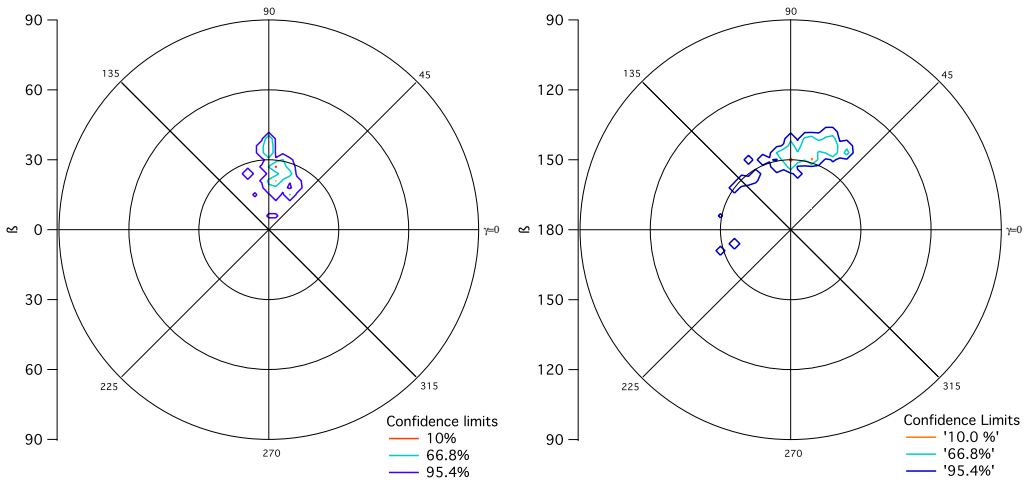

Figure S11: MCMC orientation analysis for myrG55 using the full-length GRASP55 structure with added peptide (optimized for membrane association of the N- and C- termini).

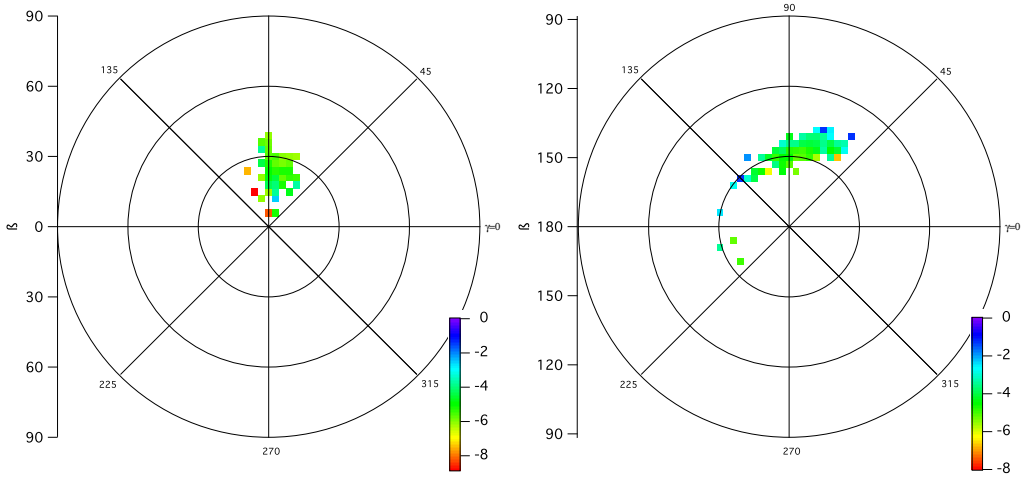

Figure S12: MCMC orientation maps of the myrG55 penetration depth into the lipid bilayer.

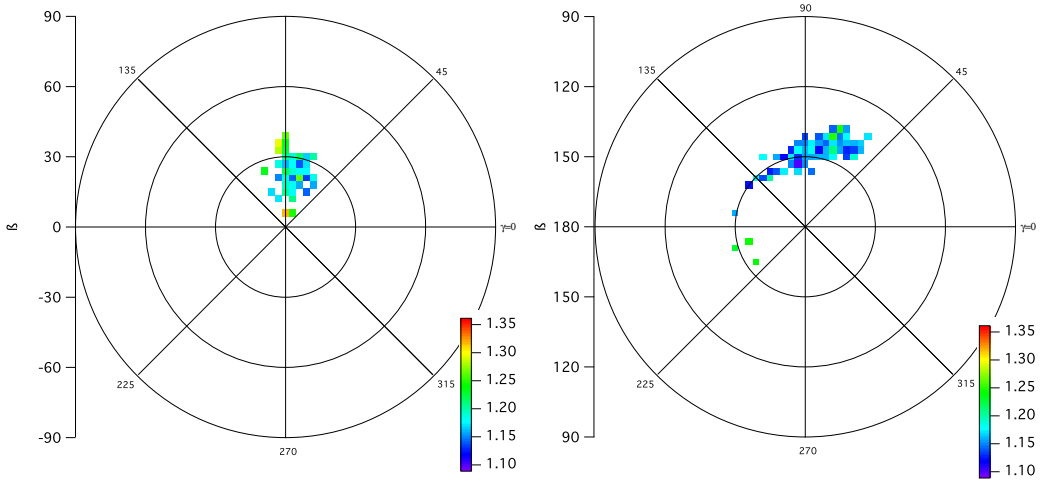

Figure S13: MCMC-derived maps of the best-fit χ2 values for the G55 orientations shown in Fig. S11.